Catalysis Science & Technology

PAPER

View Article Online
View Journal



Cite this: DOI: 10.1039/c5cy00953g

# Asymmetric epoxidation of unfunctionalized olefins accelerated by thermoresponsive self-assemblies in aqueous systems

Yaoyao Zhang,[a] Rong Tan,*[a] Guangwu Zhao,[a] Xuanfeng Luo[a] and Donghong Yin*[ab]

Received 25th June 2015,
Accepted 6th August 2015

DOI: 10.1039/c5cy00953g

www.rsc.org/catalysis

A novel thermoresponsive surfactant-type chiral salen $Mn^{III}$ catalyst was developed by axially grafting "smart" poly(*N*-isopropylacrylamide) (PNIPAAm) onto the metal center of a neat chiral salen $Mn^{III}$ complex. Characterization data suggests thermoresponsive micellization behavior of the obtained catalyst in water. The chiral metallomicellar catalyst acted as a nanoreactor to carry out asymmetric epoxidation of unfunctionalized olefins in water and dramatically accelerated reaction rates. Outstanding catalytic efficiency was observed in the nanoreactor system. In particular, quantitative conversion (99%) of styrene with high enantioselectivity (39%) was achieved over 0.8 mol% of the catalyst within 3 min, giving an unprecedented TOF value ($2.48 \times 10^3$ $h^{-1}$) which is significantly higher than that obtained over previously reported homogeneous or heterogeneous systems. Moreover, the catalyst could be easily recovered by thermocontrolled separation and reused with high activity for five cycles.

## Introduction

Asymmetric epoxidation of unfunctionalized alkenes catalyzed by chiral salen $Mn^{III}$ complexes is of great importance in synthetic organic chemistry, since the obtained enantiopure epoxides are useful chiral intermediates for synthesizing fine chemicals and several pharmaceuticals.[1–6] Industrial practice however is limited to the use of volatile dichloromethane as a solvent which often results in environmental problems. Reactions using water as a reaction medium are attracting much attention, because water is inexpensive, safe and environmentally benign.[7–11] More importantly, water often exerts a synergistic effect on chemical reactivity and selectivity.[12,13] While, to the best of our knowledge, few reports have focused on efficiently performing this transformation in water because of the insolubility of substrate and catalyst. An efficient way to address this issue is to introduce surfactant additives or to use surfactant-like catalysts.[14–16] Generally, amphiphilic surfactants can self-assemble in water *via* the interaction between hydrophobic blocks, spontaneously forming micelles with hydrophilic surfaces and hydrophobic cores. Hydrophobic reactants are concentrated within the core through hydrophobic affinity, resulting in the observed acceleration in reaction rate.[14,17–21] The pre-organizing function of surfactants in aqueous organic reactions encouraged us to envisage that a surfactant-type chiral salen $Mn^{III}$ complex obtained by introducing a hydrophilic block to a chiral salen $Mn^{III}$ complex should efficiently catalyze the asymmetric epoxidation of alkenes in water. Upon self-assembly, the hydrophobic chiral salen $Mn^{III}$ complex segment confined in the core domain can be forced into highly dense arrangements. The hydrophobic affinity of the core for reactants also favors the migration of hydrophobic substrates from an aqueous medium. A high concentration of catalyst and substrate localized within a confined hydrophobic space was expected to accelerate the asymmetric epoxidation.

However, traditional micelles are difficult to recover from solution due to their amphiphilic nature. An ideal solution to this problem is to develop "stimuli-responsive" micelles that can undergo inverse solubility changes in response to local environment changes. Temperature sensitivity is one of the most interesting properties of "stimuli-responsive" micelles. Polymeric *N*-isopropylacrylamide (PNIPAAm), with the lower critical solution temperature (LCST, 32 °C) close to room temperature, is an attractive thermoresponsive polymer.[22–25] The thermoresponsive behavior, and that it is able to undergo hydrophilic-to-hydrophobic transformation as temperature increases, make it a promising modifier in fabricating a thermoresponsive surfactant-type chiral salen $Mn^{III}$ complex for the asymmetric epoxidation of alkenes in water. At the reaction temperature (2 °C), the catalyst incorporating the hydrophobic chiral salen $Mn^{III}$ complex along with the hydrophilic PNIPAAm moiety behaves as a surfactant to form

[a] *Key Laboratory of Chemical Biology and Traditional Chinese Medicine Research (Ministry of Education), Key Laboratory of the Assembly and Application for Organic Functional Molecules, Hunan Normal University, Changsha, Hunan, 410081, China. E-mail: yiyangtanrong@126.com (R. Tan), yindh@hunnu.edu.cn (D. Yin); Fax: +86 731 8872531; Tel: +86 731 8872576*
[b] *Technology Center, China Tobacco Hunan Industrial Corporation, No. 426 Laodong Road, Changsha, Hunan, 410014, China*

a micelle-based nanoreactor in water. After the reaction, it can reversibly switch to a double hydrophobic block once heated above its LCST, leading to collapse and precipitation of the catalyst for facile recovery. This switchable behavior allows for a typical homogeneous reaction coupled with heterogeneous separation in the aqueous asymmetric epoxidation.

Herein, a thermoresponsive surfactant-type chiral salen $Mn^{III}$ complex (denoted as **catalyst 1**) was prepared by axially grafting thermoresponsive PNIPAAm onto the metal center of a neat chiral salen $Mn^{III}$ complex under basic conditions. The axial grafting mode, which does not need to tune the structures of chiral salen $Mn^{III}$ and PNIPAAm moieties, not only represents a simple and facile process, but also minimizes the formation of undesired inactive dimeric μ-oxo-manganese(IV) dimers due to steric crowding at the metal center. It has been proven that the catalyst could self-assemble to form a nanoreactor in the asymmetric epoxidation of unfunctionalized olefins in water, dramatically accelerating the aqueous epoxidation. Furthermore, it could be easily recovered from the reaction system through thermocontrolled separation. Activity switching was repeatable even after five heating/cooling cycles. Thus, the problems associated with the mass transfer and recovery limitation of the chiral salen $Mn^{III}$ complex in the asymmetric epoxidation of unfunctionalized olefins in water can be resolved.

## Experimental section

### Materials and reagents

*N*-Isopropylacrylamide (NIPAAm) was provided by Acros, and was purified by recrystallization from *n*-hexane and dried at 25 °C *in vacuo*. *N*,*N*-Azobis(isobutyronitrile) (AIBN), 2-aminoethanethiol hydrochloride and L(+)-tartaric acid were also purchased from Acros. 2-*tert*-Butyl phenol was purchased from Alfa Aesar. Pyridine-*N*-oxide (PyNO) was bought from Aldrich. Indene and 1,2-dihydronaphthalene were obtained by TCI. Other commercially available chemicals were laboratory grade reagents from local suppliers. All solvents employed in the reactions were distilled from appropriate drying agents prior to use. Organic solutions were concentrated under reduced pressure on a rotary evaporator. Styrene and indene were passed through a pad of neutral alumina before use. Amino-terminated PNIPAAm (PNIPAAm-$NH_2$) was prepared by radical polymerization using thiol compounds as a chain transfer agent according to the procedure described in the literature.[26] The neat complex of [(*R*,*R*′)-(*N*,*N*′-bis(3,5-di-*tert*-butylsalicylidene)-1,2-cyclo-hexanediaminato] manganese(III)–chloride was prepared according to the described procedure.[27]

### Methods

Number-average molecular weight ($M_n$) of PNIPAAm was obtained by gel permeation chromatography (GPC). Analyses were performed on an Alltech Instrument (Alltech, America) using THF as the solvent eluting at a flow of 1 mL $min^{-1}$ through a Jordi GPC 10 000 A column (300 mm × 7.8 mm) equipped with an Alltech ELSD 800 detector. The system was calibrated with standard polystyrenes. The detection temperature is 40 °C and column temperature is 30 °C. $^1H$ NMR spectra of samples were recorded on a Varian-500 spectrometer. FT-IR spectra were obtained as potassium bromide pellets with a resolution of 4 $cm^{-1}$ and 32 scans in the range 400–4000 $cm^{-1}$ using an AVATAR 370 Thermo Nicolet spectrophotometer. UV-vis spectra of the complex were recorded on a UV-vis Agilent 8453 spectrophotometer at 300–600 nm. The lower critical solution temperature (LCST) of the thermoresponsive chiral salen $Mn^{III}$ complex in water was measured by transmittance using a UV-visible photometer. The concentration of the complex is 1 wt%. The rising temperature ratio is 5 °C $min^{-1}$. X-ray Photoelectron Spectroscopy (XPS) data were obtained with an ESCALab220i-XL electron spectrometer from VG Scientific using 300 W Al Kα radiation. The base pressure was about $3 \times 10^{-9}$ mbar ($3 \times 10^{-7}$ Pa). The manganese content in the catalyst was determined by inductively coupled plasma-atomic emission spectrometry (ICP-AES) on a BAIRD PS-6 analyzer, after the sample was dissolved in deionized water. The optical rotation of the catalysts was measured in dichloromethane on a WZZ-2A Automatic Polarimeter. The surface tension of an aqueous solution of **catalyst 1** was measured as a function of catalyst concentration ($3.75 \times 10^{-2}$–500.0 mmol $L^{-1}$) on a Krüss K12 tensiometer using the Wilhelmy plate method at 25 °C. The surface tension *vs.* catalyst concentration plot gives information on the critical micelle concentration (CMC). Morphological observation of the micelles was performed by TEM on a Microscope JEM-2100F at an accelerating voltage of 200 kV. The sample was prepared by depositing an aqueous solution of **catalyst 1** (0.5 mg $mL^{-1}$) onto a carbon-coated copper grid, followed by the removal of excess solution by blotting the grid with filter paper. The samples were dried for 72 h at room temperature in a desiccator containing dried silica gel. After that, the samples were negatively stained by phosphotungstic acid and dried for another 72 h before examination. The average hydrodynamic diameter and size distribution of the self-assembled aggregates were determined by dynamic light scattering (DLS) using a MS2000 Laser Particle Size Analyzer (Malvern, UK). The concentration of the sample was 0.5 mg $mL^{-1}$. Light transmittance was fixed at 633 nm with a scattering angle of 90°.

### Preparation of catalyst 1

The preparation of **catalyst 1** is outlined in Scheme 1.

**Synthesis of PNIPAAm-$NH_2$.** NIPAAm (50 mmol), 2-aminoethanethiol hydrochloride (1 mmol) and AIBN (0.5 mmol) were dissolved in 20 mL of methanol in a Schlenk tube. The reaction mixture was degassed by bubbling with nitrogen gas at room temperature for 30 min, and polymerization was carried out at 70 °C for 5 h under a $N_2$ gas atmosphere. The mixture was cooled to room temperature, and then treated with

 

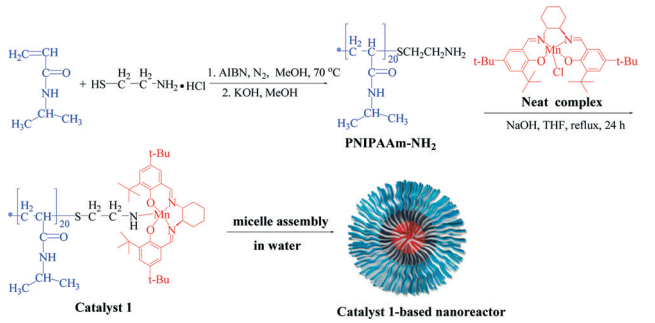


**Scheme 1** Schematic representation of synthesis and self-assembly of surfactant-type **catalyst 1**.

KOH (1 mmol). The obtained solution was concentrated under vacuum and then poured into diethyl ether to precipitate the polymer. The crude product was further purified by repeated precipitation from a THF solution into diethyl ether to remove unreacted monomers, and then dried for 12 h under a vacuum at 25 °C to give a white solid of PNIPAAm-$NH_2$. FT-IR (KBr): $\gamma_{max}/cm^{-1}$ 3438, 3309, 3072, 2974, 2931, 2878, 2825, 1652, 1541, 1458, 1387, 1367, 1261, 1173, 1130, 1055, 987, 928, 881, 839, 633, 517 $cm^{-1}$. $^1H$ NMR (500 MHz, $D_2O$): $\delta$ 3.89 (s, 20H), 2.92 (s, 12H), 2.62 (s, 1H), 2.44 (s, 1H), 2.00 (s, 20H), 1.57 (s, 42H), 1.14 (s, 123H). The $M_n$ of the PNIPAAm-$NH_2$ was *ca.* 2300 g $mol^{-1}$, which was measured by GPC using conventional calibration with PS standards. Thus, the polymer was composed of *ca.* 20 repeating units of NIPAAm monomer.

**Synthesis of catalyst 1.** A solution of neat chiral salen $Mn^{III}$ complex (2.7 mmol, 1.71 g), PNIPAAm-$NH_2$ (2.5 mmol) and an adequate amount of sodium hydroxide in THF (50 mL) was vigorously stirred for 24 h under reflux. After removing THF, the residue was purified by precipitation from diethyl ether (3 × 50 mL) and dried *in vacuo* at 25 °C to get the thermoresponsive surfactant-type catalyst (denoted as **catalyst 1**). FT-IR (KBr): $\gamma_{max}/cm^{-1}$ 3309, 3072, 2974, 2931, 2878, 1652, 1541, 1458, 1387, 1365, 1254, 1173, 1130, 928, 879, 837, 644, 571, 507, 424 $cm^{-1}$. UV-vis ($CH_2Cl_2$): $\lambda_{max}/nm$ ($\varepsilon_{max}$/L $mol^{-1}$ $cm^{-1}$) 322 (148 162), 429 (32 119), 502 (5963). Mn ion content: 0.33 mmol $g^{-1}$ (theoretical value: 0.34 mmol $g^{-1}$). $\alpha_D^{25}$ = +168 ($C$ = 0.02 in $CH_2Cl_2$). The LCST of **complex 1** in aqueous solution was *ca.* 35 °C, which was determined by transmittance measurements using the UV-vis spectrophotometer.

### Catalyst testing

Unfunctionalized alkene (0.25 mmol) and PyNO (0.5 mmol, 0.048 g) were added into the solution of catalyst (0.8 mol% of substrate, based on Mn content) in water (1 mL) at 2 °C. Buffered NaOCl as an oxidant (0.5 mmol, 0.5 M, pH = 11.5) was then added in one portion under stirring. The reaction was monitored constantly by TLC. After achieving the desired epoxidation level, the reaction mixture was heated to 40 °C. Catalyst was precipitated out from the reaction system, washed with *n*-hexane (3 × 5 mL), dried in a vacuum, and finally recharged with fresh substrate, additive, and oxidant for the next catalytic cycle. The supernatants separated from the reaction system were extracted with *n*-hexane thrice. Further purification of the collected *n*-hexane phase by flash column chromatography afforded epoxides. The conversion and enantiomeric excess (ee) were determined by a 6890 N gas chromatograph (Agilent Co.) equipped with the chiral capillary column (HP19091G-B213, 30 m × 0.32 mm × 0.25 μm) and a FID detector. Nitrogen was used as the carrier gas with a flow of 30 mL $min^{-1}$. The injector temperature was 250 °C, and the detector temperature was also 250 °C. The retention times of the corresponding chiral epoxides ($t_{absolute\ configuration}$) are as follows: (a) styrene epoxide: the column temperature was 100 °C, major enantiomer $t_R$ = 7.1 min and minor enantiomer $t_S$ = 7.6 min; (b) α-methylstyrene epoxide: the column temperature was 100 °C, major enantiomer $t_R$ = 8.0 min and minor enantiomer $t_S$ = 7.7 min; (c) indene epoxide: the column temperature was programmed from 80 to 180 °C with 5 °C $min^{-1}$. Major enantiomer $t_{RS}$ = 11.9 min and minor enantiomer $t_{SR}$ = 11.5 min; (d) 1,2-dihydronaphthalene epoxide: the column temperature was programmed from 80 to 180 °C with 5 °C $min^{-1}$. Major enantiomer $t_{RS}$ = 19.4 min and minor enantiomer $t_{SR}$ = 18.8 min; (e) 6-nitro-2,2′-dimethylchromene epoxide: the column temperature was programmed from 80 to 200 °C with 3 °C $min^{-1}$ and retained at 200 °C for 5 min. Major enantiomer $t_{RR}$ = 30.8 min and minor enantiomer $t_{SS}$ = 30.3 min; (f) 6-cyano-2,2′-dimethylchromene epoxide: the column temperature was programmed from 80 to 200 °C with 4 °C $min^{-1}$. Major enantiomer $t_{RR}$ = 24.3 min and minor enantiomer $t_{SS}$ = 24.0 min.

### Epoxidation reaction for kinetics measurements

A cooled solution of **catalyst 1** in water (1 mL) was stirred with styrene (0.25 mmol). Buffer NaOCl (0.5 mmol, 1 mL, pH = 11.5) was then added into the stirred solution in one portion at 2 °C. To determine the rate of epoxidation, aliquots at an interval of 1 min were drawn from the reaction mixture, quenched with triphenylphosphine, and analyzed by GC.

## Results and discussion

### Preparation and characterization of catalysts

Nanometer-scale reactors that mimic enzyme-based reaction compartments have drawn much attention in recent years, since they provide an opportunity to perform organic reactions "in water".[28–31] Surfactant-type catalysts can spontaneously self-assemble in water to form micelle-based nanoreactors, and hopefully accelerate the aqueous organic reaction.[15,32] Therefore, we decided to develop a surfactant-type chiral salen $Mn^{III}$ complex for efficient asymmetric epoxidation of unfunctionalized alkenes in water. PNIPAAM with inverse temperature-dependent water solubility was introduced into the structure of the chiral salen $Mn^{III}$ complex for this development. Axial grafting mode, a common way to heterogenize a chiral salen $Mn^{III}$ complex which does not

need tuning of the structure of the chiral salen $Mn^{III}$ complex,[33] was employed for this modification. It not only represents a simple and facile process, but also ensures effective site isolation due to steric crowding at the metal center, since catalyst density and site isolation are the key issues in giving extremely active and selective chiral salen $Mn^{III}$ catalysts.[33] The synthesis route for the thermoresponsive catalyst is outlined in Scheme 1. Amino-terminated PNIPAAm, prepared by radical polymerization using thiol compounds as a chain transfer agent, directly reacted with the neat chiral salen $Mn^{III}$ complex under basic conditions, affording **catalyst 1**.

## Characterization of samples

**FT-IR.** The obtained **catalyst 1**, as well as the PNIPAAm and neat chiral complex for comparison, were characterized by FT-IR spectra (Fig. 1). PNIPAAm exhibits characteristic vibration bands at around 3309 $cm^{-1}$ (–NH of –CONH–), 3072 $cm^{-1}$ (CH of –CH–CH–), 2974, 2931 $cm^{-1}$ (–$CH_3$ of –CH $(CH_3)_2$), 2878 $cm^{-1}$ (CH of –CH $(CH_3)_2$) and 1652 $cm^{-1}$ (–C═O of –CONH–) (Fig. 1a) in the FT-IR spectrum.[34] Upon grafting, new characteristic bands at around 1251, 571, and 424 $cm^{-1}$ appear along with the characteristic vibration bands associated with PNIPAAm (Fig. 1b), which are assigned to the characteristic vibrations of Ph–O, Mn–O, and Mn–N in the salen $Mn^{III}$ unit,[35–37] respectively. Obviously, the structure of chiral salen $Mn^{III}$ complex is maintained in **catalyst 1**. Notably, the characteristic vibrations of Mn–O and Mn–N shifted from 565 and 413 $cm^{-1}$ to 571 and 424 $cm^{-1}$, respectively, after grafting, compared with those of the neat chiral salen $Mn^{III}$ complex (Fig. 1b *vs.* c). This slight shift should account for the interaction between the metal center of the chiral salen $Mn^{III}$ complex and the amino-terminated PNIPAAm. It is the interaction that is responsible for axially bonding PNIPAAm-$NH_2$ to the chiral salen $Mn^{III}$ complex.

**UV-vis.** UV-vis spectra of neat complex and **catalyst 1** in dichloromethane furthermore verified the interaction between the metal center of the chiral salen $Mn^{III}$ complex and the amino-terminated PNIPAAm, as described in Fig. 2. Obviously, the neat complex exhibited the characteristic peaks at around 325, 438 and 509 nm (Fig. 2a), which are due to the charge transfer transition of the salen ligand, the metal-to-ligand charge-transfer transition and the d–d transition of the complex, respectively.[35] As for **catalyst 1**, the corresponding characteristic peaks shifted to 322, 429 and 502 nm, respectively (Fig. 2a *vs.* b). It was logical to relate the blue shift with the electronegative nitrogen atom bonded on the manganese center in **catalyst 1**. A similar deduction has also been made by Huang *et al.*[38,39] They reported axial N–Mn bonding between chiral salen $Mn^{III}$ complexes and amine (–$NH_2$) group modified supports. These observations provided a direct proof for the presence of N–Mn bonding in **catalyst 1**. PNIPAAm was thus axially appended on the manganese center of the chiral salen $Mn^{III}$ complex through the terminal amine (–$NH_2$) group, which not only acted as a thermoresponsive inductor to switch on and off the nanoreactor, but also behaved as a bulk axial group to ensure the necessary isolation of the active site.

**XPS.** The binding behavior can also be confirmed by characterizing the neat complex and **catalyst 1** using XPS, since the electronic environment influences the binding energy of the core electrons of the metal. XPS spectra obtained from the neat complex and **catalyst 1** are shown in Fig. 3. The neat complex exhibits a $Mn2p_{3/2}$ core level peak at a binding energy of 642.0 eV, in accordance with an earlier literature value.[40] While, the binding energy slightly increases to 642.4 eV in the case of **catalyst 1**. The observed increase in the binding energy should be attributed to the formation of the N–Mn bond in **catalyst 1**, which affected the electronic environment of the manganese center. A similar observation has also been made for a chiral salen $Mn^{III}$ catalyst which was axially grafted on an amine (–$NH_2$) group modified support through N–Mn bonding.[41]

**CMC determination.** CMC is one of the most useful parameters for surfactant-type **catalyst 1**, since the catalyst can self-assemble to form micelles above the CMC.[42] Surface

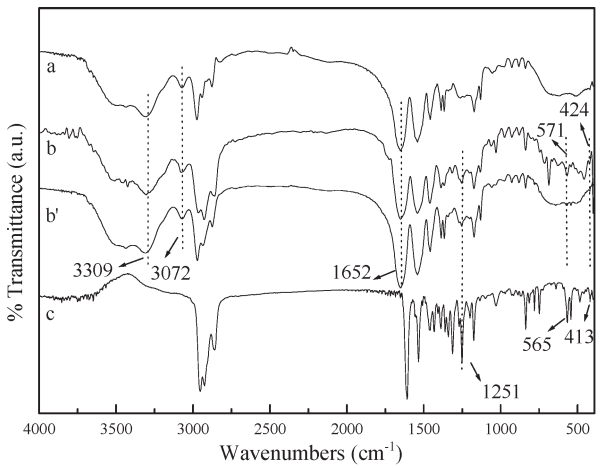


Fig. 1 FT-IR spectra of PNIPAAM (a), fresh **catalyst 1** (b), recovered **catalyst 1** after the 5th reuse (b′) and neat complex (c).

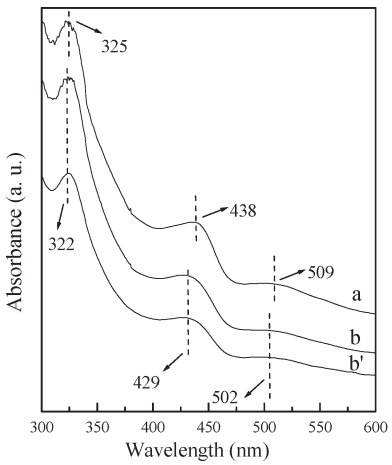


Fig. 2 UV-vis spectra of neat complex (a), fresh **catalyst 1** (b) and recovered **catalyst 1** after the 5th reuse (b′).

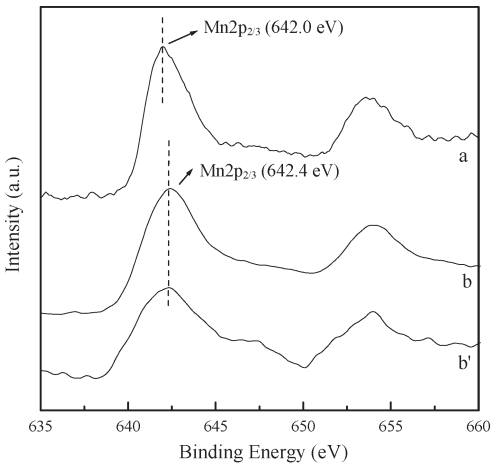


Fig. 3 Mn $2p_{2/3}$ XPS spectra of neat complex (a), fresh **catalyst 1** (b) and recovered **catalyst 1** after the 5th reuse (b′).

tension measurements over a wide range of concentrations were used in the CMC determination. Fig. 4 shows the surface tension *versus* logarithm of concentration plots for **catalyst 1** in water at 25 °C. Clearly, the surface tension decreased dramatically as the concentration of **catalyst 1** increased. There was an inflection point at the characteristic concentration of 0.5 mmol $L^{-1}$. And the surface tension does not change substantially as a function of concentration of **catalyst 1** above 0.5 mmol $L^{-1}$. Therefore, the CMC of **catalyst 1** is 0.5 mmol $L^{-1}$, above which, **catalyst 1** could self-assemble in water to form micelles.

## Morphological analyses

A TEM measurement was employed to observe the morphology of the micelles, as shown in Fig. 5. Obviously, **catalyst 1** self-assembled in water to form spherical aggregates with an average diameter of *ca.* 9 nm, as confirmed by TEM. The high dispersion of the aggregates suggests the stability of micelles in water. In order to further determine the hydrodynamic diameter and size distribution the self-assembled aggregates, **catalyst 1** in water (0.5 mg $mL^{-1}$) was analyzed by a MS2000 Laser Particle Size Analyzer (Fig. 6). Indeed, the micelles show a narrow diameter distribution with an average

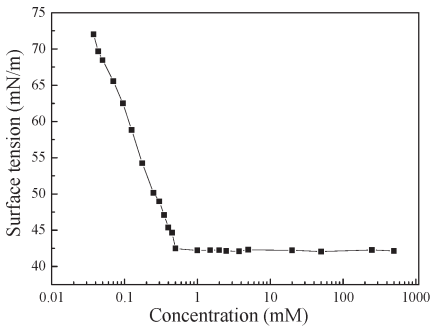


Fig. 4 Plot of surface tension against logarithm of concentration for **catalyst 1** in water at 25 °C.

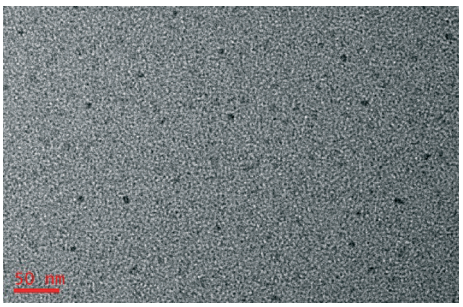


Fig. 5 TEM micrograph of self-assembled **catalyst 1** stained with phosphotungstic acid.

diameter of 78 nm. Notably, the size obtained from DLS is much greater than that from TEM (*ca.* 9 nm), probably due to the swelling of surface PNIPAAM in aqueous solution. In fact, DLS allows determination of the hydrodynamic diameter of the micelles in water, whereas TEM shows the dehydrated solid state of the dried micelles. Furthermore, homogeneous distribution and spherical morphology of the self-assemblies led to a small polydispersity index (PDI) value of 0.282.[43]

## LCST determination

The thermal sensitivity of these micelle structures was measured *via* spectrophotometry by determining the turbidity of a solution at various temperatures (Fig. 7). A sharp decrease in transmittance occurred at *ca.* 35 °C, which signified a hydrophilic-to-hydrophobic phase transition of the PNIPAAm block (Fig. 7a). Therefore, **catalyst 1**-based micelles were formed when the local temperature was below 35 °C and disaggregated at temperatures above 35 °C. Furthermore, the LCST of **catalyst 1** (35 °C) was 3 °C higher than that for PNIPAAm (32 °C) (Fig. 7a *vs.* 7b). This trend may be attributed to the interaction between the chiral salen $Mn^{III}$ complex moiety and the PNIPAAm component.

## Catalytic performances

The **catalyst 1**-based micelles behave as catalytic nanoreactors for the asymmetric epoxidation of alkenes in water. Styrene was chosen as a model substrate to investigate the catalytic

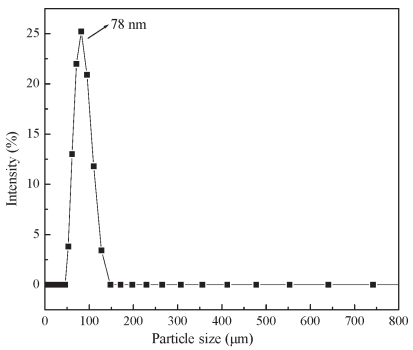


Fig. 6 Hydrodynamic diameter of self-assembled **catalyst 1** (PDI = 0.282).

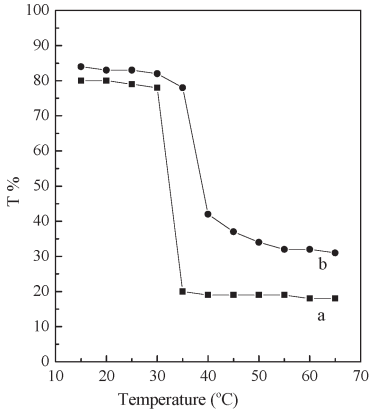


**Fig. 7** Plot of the changes in solution transmittance as a function of temperature for PNIPAAm (a) and **catalyst 1** (b) solution in water. The turbidimetry curve is drawn by measuring the transmittance ($\lambda_{max}$ = 450 nm) of the corresponding aqueous polymer solution at a fixed concentration (5 mg $mL^{-1}$) as a function of temperature. The LCST corresponds to the mid-point of the transition curve.

performance of **catalyst 1** in pure water. All catalytic reactions were conducted at 2 °C to ensure the formation of a nanoreactor with a hydrophilic surface and a hydrophobic catalytic core during the reaction. The results are presented in Table 1.

As expected, **catalyst 1** was extremely efficient for the asymmetric epoxidation of styrene in water. Quantitative conversion (99%) with high enantioselectivity (ee, 39%) was achieved with 0.8 mol% of **catalyst 1** within 3 min (Table 1, entry 1). While only a 16% conversion of styrene with a 5% ee value was obtained over the neat complex under identical conditions (Table 1, entry 3). Notably, PNIPAAm alone was inactive (Table 1, entry 4). Therefore, the unprecedented acceleration in reaction rate (six times faster than the neat complex) should relate to the micellization behavior of **catalyst 1** in the reaction system. During the reaction, **catalyst 1** containing hydrophobic and hydrophilic blocks spontaneously self-assembled in water to form micelles with a hydrophobic catalytic core and a hydrophilic surface. The hydrophobic core provided a hydrophobic microenvironment with a high local concentration of catalytic sites along with the concentrated hydrophobic substrates, while the hydrophilic surface guaranteed water-solubility of the aggregate. The "concentration effect" of the nanoreactor resulted in the observed acceleration in the reaction rate. Moreover, the remarkable enhancement of the reaction rate might also be attributed to the phase-transfer capability of surfactant-type **catalyst 1**, which transported the real oxidant HClO from the surrounding aqueous environment to the hydrophobic core for faster catalysis. An unprecedented TOF value ($2.48 \times 10^3$ $h^{-1}$) was achieved over **catalyst 1** in the aqueous epoxidation of styrene. The value was even significantly higher than that obtained over previously reported chiral salen $Mn^{III}$ complexes in homogeneous or heterogeneous systems.[41,44–47] Furthermore, in the absence of the additive PyNO, the activity and enantioselectivity of **catalyst 1** apparently decreased, indicating that PyNO as an axial ligand had a pronounced effect on both the activity and the enantioselectivity of the asymmetric epoxidation reaction, which has been reported for other chiral salen Mn(III) catalysts (Table 1, entry 2).[41]

**Table 1** Results of the enantioselective epoxidation of unfunctionalized olefins over different chiral salen $Mn^{III}$ complexes in water[a]

| Entry | Catalyst | Substrate | Product | $t$ (min) | Conv.[b]/% | ee[b]/% | TOF[c] × $10^3$ $h^{-1}$ |
|---|---|---|---|---|---|---|---|
| 1 | **Catalyst 1** |  |  | 3 | 99 | 39 | 2.48 |
| 2 | **Catalyst 1**[d] | | | 3 | 45 | 27 | 1.13 |
| 3 | Neat complex | | *R* | 3 | 16 | 5 | 0.40 |
| 4 | PNIPAAm | | | 3 | trace | / | / |
| 5 | **Catalyst 1** |  |  | 3 | 48 | 49 | 1.20 |
| 6 | **Catalyst 1** | | | 30 | 99 | 75 | / |
| 7 | Neat complex | | *R* | 3 | 15 | 35 | 0.38 |
| 8 | **Catalyst 1** |  | 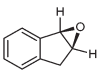 | 3 | 45 | 47 | 1.13 |
| 9 | **Catalyst 1** | | | 35 | 99 | 70 | / |
| 10 | Neat complex | | *1R, 2S* | 3 | 12 | 40 | 0.30 |
| 11 | **Catalyst 1** |  |  | 3 | 40 | 51 | 1.00 |
| 12 | **Catalyst 1** | | | 45 | 99 | 77 | / |
| 13 | Neat complex | | *1R, 2S* | 3 | 10 | 44 | 0.25 |
| 14 | **Catalyst 1** | 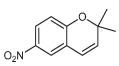 | 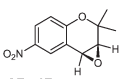 | 3 | 16 | 83 | 0.40 |
| 15 | **Catalyst 1** | | | 180 | 99 | 92 | / |
| 16 | Neat complex | | *3R, 4R* | 3 | 3 | 78 | 0.08 |
| 17 | **Catalyst 1** | 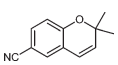 | 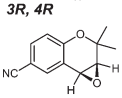 | 3 | 14 | 80 | 0.35 |
| 18 | **Catalyst 1** | | | 200 | 99 | 94 | / |
| 19 | Neat complex | | *3R, 4R* | 3 | 7 | 76 | 0.18 |

[a] Catalyst (0.8 mol% of substrate, based on manganese ion content), substrate (0.25 mmol), pyridine *N*-oxide (0.5 mmol), NaClO (0.5 mmol, 0.5 M, pH = 11.5, added in one portion), water (1 mL), 2 °C. [b] Determined by GC. [c] TOF = (moles of substrate converted)/(moles of manganese centers) per hour, calculated from 3 min conversions. [d] Without PyNO.

To further understand the acceleration effect of **catalyst 1** in aqueous reaction systems, kinetics was used to study the reaction rates of asymmetric epoxidation of styrene over various amounts of **catalyst 1** in water. The catalyst amount was reduced from 0.8 to 0.1 mol%. Time-dependent plots of styrene conversion with various amounts of **catalyst 1** are shown in Fig. 8A. Both reactions in water reached equilibrium within 3 min. Notably, the conversion of styrene linearly increased up to 1 min, after which a significant increase was not observed. Therefore, the initial rate constant $k_{obs}$ values were determined from the data within this time range. Detailed kinetic data for the catalyst amount-dependence in water are given in Fig. 8C-a. Obviously, reaction rates decreased with the reduction in catalyst amount in water, in terms of initial rate constants $k_{obs}$. By reducing the amount of **catalyst 1** from 0.8 to 0.4 mol%, the $k_{obs}$ value decreased smoothly (Fig. 8C-a). It was logical that lower catalyst amount should reduce the total number of nanoreactors in solution and hence less "catalytic pumps" to catalyze the aqueous organic reaction. While, further lowing the catalyst amount to 0.2 mol%, led to a sharp decrease in the $k_{obs}$ value (Fig. 8C-a). In particular, a $k_{obs}$ value of only 17.0 M $min^{-1}$ was obtained when the catalyst amount was reduced to 0.1 mol% (Fig. 8A-e). The decrease in reaction rate could be caused by the limited amount of available **catalyst 1** to form nanoreactors in water for confined catalysis. Therefore, **catalyst 1** self-assembles to form micelles in aqueous reaction systems when the catalyst amount is above 0.4 mol%. Interestingly, this value (0.4 mol% of substrate in 2 mL solvent) agrees with the CMC (0.5 mmol $L^{-1}$) of **catalyst 1**. Notably 0.8 mol% of **catalyst 1**-based micelles in water were sufficient for affording a quantitative conversion (99%) of styrene with a high ee value (39%) (Fig. 8A-a).

For comparison, we also used kinetics to study the reaction rates of asymmetric epoxidation of styrene over various amounts of **catalyst 1** in dichloromethane, as shown in Fig. 8B. Detailed kinetics data for catalyst amount-dependence in dichloromethane are presented in Fig. 8C-b. Notably, catalysis in dichloromethane was far less efficient than that in water, in terms of corresponding initial rate constants $k_{obs}$ (Fig. 8C-b *vs.* a). And the $k_{obs}$ values in dichloromethane decreased smoothly with the reduction in catalyst amount from 0.8 to 0.1 mol% (Fig. 8C-b). Actually, dichloromethane is a good solvent for the blocking of the chiral salen $Mn^{III}$ complex. Hence, **catalyst 1** containing a hydrophilic PNIPAAM group and a hydrophobic complex moiety may locate at the interface of water (aqueous NaClO) and dichloromethane in the biphasic system. Self-assembly into micelles didn't occur. **Catalyst 1** thus behaved as a common phase-transfer catalyst, rather than a concentrator. Lower local concentration of the reagent and catalytic species in the common organic system was unfavorable for efficient catalysis.

Enhanced reaction rate over **catalyst 1** is also noticeable in the case of α-methylstyrene, indene, 1,2-dihydronaphthalene, 6-cyano-2,2-dimethylchromene, and 6-nitro-2,2-dimethylchromene, as shown by TOF in Table 1. **Catalyst 1** gave significantly higher TOF values than the neat complex in corresponding epoxidations, due to the ability of the hydrophobic micelle cores to effectively sequester the organic substrates from the surrounding aqueous environment (Table 1, entry 5 *vs.* 7, entry 8 *vs.* 10, entry 11 *vs.* 13, entry 14 *vs.* 16, and entry 17 *vs.* 19). But unfortunately, the **catalyst 1**-based nanoreactor showed substrate selectivity based on the size of substrates. Despite still being unfunctionalized alkenes, bulkier alkenes were less reactive than styrene during aqueous asymmetric epoxidation (Table 1, entries 5, 8 and 11 *vs.* entry 1). In the presence of 0.8 mol% of **catalyst 1**, α-methylstyrene, indene, and 1,2-dihydronaphthalene only gave 40–48% conversions with unsatisfactory ee values. For more sterically hindered alkenes, such as 6-nitro-2,2-dimethylchromene and 6-cyano-2,2-dimethylchromene, even lower conversions (14–16%) were obtained during the reaction (Table 1, entries 14 and 17). While, the difference in the reactivity of the alkenes was not obvious when the neat complex was used as the catalyst (Table 1, entries 3, 7, 10 and 13). This type of substrate selectivity should account for the selective shell permeability.[48] Nanostructured shells consisting of bulky PNIPAAm segments acted as a size-exclusion gate in the nanoreactor, which favored the penetration of small alkenes into the catalyst-containing micelle core for more efficient catalysis. In particular, substituted 2,2-dimethylchromene molecules are solid and insoluble in water, which consequently have difficulty permeating into the hydrophobic core of the nanoreactors for efficient catalysis (Table 1, entries 14 and 17). This gated permeability behavior makes the **catalyst 1**-based micelle a selective nanoreactor for the asymmetric epoxidation of alkenes in water. Notably, all alkenes used in this work get quantitatively oxidized to the corresponding epoxides with good to excellent enantioselectivity in water, in the case of prolonged reaction time (Table 1, entries 6, 9, 12, 15 and 18). The results suggested the flexibility of **catalyst 1** in green asymmetric epoxidation. It is the first successful

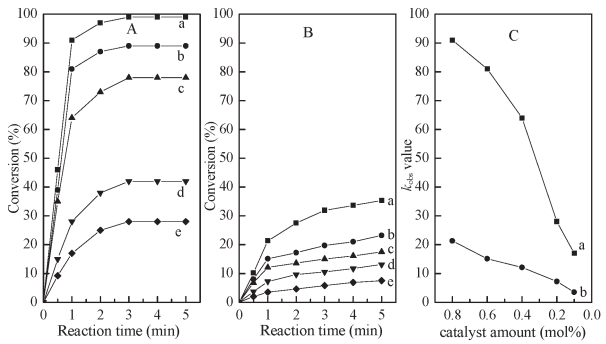


**Fig. 8** Time-dependent plots of styrene conversion with various amounts of **catalyst 1** in water (A) and in dichloromethane (B) (catalyst amount based on manganese ion content: 0.8 mol% (a), 0.6 mol% (b), 0.4 mol% (c), 0.2 mol% (d), and 0.1 mol% (e)), and detailed $k_{obs}$ values for catalyst amount-dependence (C) in water (a) and in dichloromethane (b).

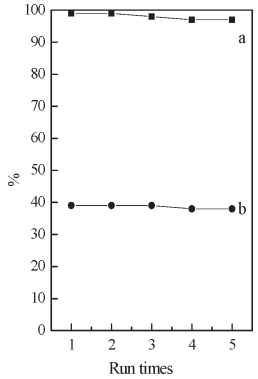


Fig. 9 Reuse of **catalyst 1** in asymmetric epoxidation of styrene with NaClO as oxidant in water at 2 °C (a: conversion; b: ee values).

example for efficiently performing asymmetric epoxidation of alkenes in pure water.

### Recycling

Apart from its high efficiency, another salient feature of **catalyst 1** in water is its "smart" recovery. After each reaction, **catalyst 1** turned to a double hydrophobic block once heated above its LCST, leading to precipitation of catalyst for the next cycle. The aqueous phase was separated from the catalyst by decantation. Notably, although *n*-hexane was used to extract a small amount of epoxide from reaction solution in the present work, this approach was expected in large-scale industrial processes, in which the organic product phase can be directly separated from water without the use of any organic solvents. To our delight, **catalyst 1** could be reused at least five times without significant loss of activity, as shown in Fig. 9.

Leaching tests of the reaction medium were performed by directly determining the manganese content in the supernatant *via* chemical analysis. No manganese was detected in the supernatant, which revealed the negligible leaching loss of manganese species during the reaction. Moreover, chemical analysis of the recovered catalyst gave manganese content (0.32 mmol $g^{-1}$) almost identical to that of the fresh one (0.33 mmol $g^{-1}$). FT-IR (see Fig. 1b *vs.* b′), UV-vis (see Fig. 2b *vs.* b′) and XPS (see Fig. 3b *vs.* b′) spectra showed no significant change in catalyst even after the 5th reuse. Therefore, the efficient **catalyst 1** was stable under the basic reaction condition (pH 11.5, NaClO buffer), and the axial N–Mn bonding remained intact during the epoxidation. Oxidative decomposition of the chiral salen $Mn^{III}$ complex, a main reason for deactivation of the complex in basic epoxidation,[41,49,50] was avoided by localizing the complex within a hydrophobic core. The possibility of the formation of undesired inactive dimeric μ-oxo-manganese(IV) dimers,[51] the cause for deactivation of the catalytic species, can also be prevented because of the bulky steric encumbrance of PNIPAAm on the manganese center. Furthermore, the mild reaction conditions used in our studies, such as extremely short reaction time and low temperature, should potentially minimize catalyst degradation.

## Conclusions

We have demonstrated the first asymmetric epoxidation of unfunctionalized olefins in pure water using a chiral salen $Mn^{III}$ complex-based thermoresponsive nanoreactor. The nanoreactor with a hydrophobic catalytic core and a hydrophilic surface exhibited some distinct characteristics as follows: (a) the hydrophobic core created a hydrophobic microenvironment with high local concentration of active sites and concentrated substrates, confining the asymmetric epoxidation for efficient catalysis; (b) the hydrophilic surface guaranteed water-solubility of the nanoreactor, circumventing the limited mass transfer associated with an aqueous organic reaction. Furthermore, the thermoresponsivity of the nanoreactor facilitated the recovery of the catalyst from the reaction system by simply adjusting the local temperature. The chiral salen $Mn^{III}$ complex-based nanoreactor thus showed extremely high catalytic efficiency and steady reusability in the asymmetric epoxidation of unfunctionalized olefins in water without the need for any organic solvents. The advantages allow for industrial practice of the asymmetric epoxidation of unfunctionalized alkenes, and also raise the prospect of making water a viable environmentally friendly medium for organic synthesis.

## Acknowledgements

The work was supported by the National Natural Science Foundation of China (Grant No. 21476069, 21003044), the Scientific Research Fund of Hunan Provincial Education Department (13B072), the Program for Excellent Talents in Hunan Normal University (ET14103), the Program for Science and Technology Innovative Research Team in Higher Educational Institutions of Hunan Province, the Foundation for Innovative Research Groups of the Hunan Natural Science Foundation of China and the Construct Program of the Key Discipline in Hunan Province.

## References

1 W. Zhang, J. L. Loebach, S. R. Wilson and E. N. Jacobsen, *J. Am. Chem. Soc.*, 1990, **112**, 2801.
2 S. Liao and B. List, *Angew. Chem., Int. Ed.*, 2009, **48**, 1.
3 S. Liao and B. List, *Angew. Chem., Int. Ed.*, 2010, **49**, 628.
4 F. Song, C. Wang and W. Lin, *Chem. Commun.*, 2011, **47**, 8256.
5 R. Luo, R. Tan, Z. Peng, W. Zheng, Y. Kong and D. Yin, *J. Catal.*, 2012, **87**, 170.
6 S. Shabbir, Y. Lee and H. Rhee, *J. Catal.*, 2015, **322**, 104.
7 B. E. Hanson, *Coord. Chem. Rev.*, 1999, **185–186**, 795.
8 U. M. Lindstrom, *Chem. Rev.*, 2002, **102**, 2751.
9 J. Tan, H. Li and Y. Gu, *Green Chem.*, 2010, **12**, 1772.
10 P. Cotanda, A. Lu, J. P. Patterson, N. Petzetakis and R. K. O'Reilly, *Macromolecules*, 2012, **45**, 2377.

 

11 Y. Kong, R. Tan, L. Zhao and D. Yin, *Green Chem.*, 2013, **15**, 2422.
12 Y. Jung and R. A. Marcus, *J. Am. Chem. Soc.*, 2007, **129**, 5492.
13 A. Chanda and V. V. Fokin, *Chem. Rev.*, 2009, **109**, 725.
14 T. Dwars, E. Paetzold and G. Oehme, *Angew. Chem., Int. Ed.*, 2005, **44**, 7174.
15 S. Luo, X. Mi, S. Liu, H. Xu and J. Cheng, *Chem. Commun.*, 2006, 3687.
16 V. Rauniyar, A. D. Lackner, G. L. Hamilton and F. D. Toste, *Science*, 2011, **334**, 1681.
17 K. Manabe, S. Iimura, X. Sun and S. Kobayashi, *J. Am. Chem. Soc.*, 2002, **124**, 11971.
18 Y. Wang, H. Xu, N. Ma, Z. Wang, X. Zhang, J. Liu and J. Shen, *Langmuir*, 2006, **22**, 5552.
19 J. Li, Y. Tang, Q. Wang, X. Li, L. Cun, X. Zhang, J. Zhu, L. Li and J. Deng, *J. Am. Chem. Soc.*, 2012, **134**, 18522.
20 A. Lu and R. K. O'Reilly, *Curr. Opin. Biotechnol.*, 2013, **24**, 639.
21 Y. Liu, Y. Wang, Y. Wang, J. Lu, V. Piñón, III and M. Weck, *J. Am. Chem. Soc.*, 2011, **133**, 14260.
22 T. Sun and G. Qing, *Adv. Mater.*, 2011, **23**, 57.
23 T. Sun, G. Qing, B. Sua and L. Jiang, *Chem. Soc. Rev.*, 2011, **40**, 2909.
24 V. B. Schwartz, F. Thétiot, S. Ritz, S. Pütz, L. Choritz, A. Lappas, R. Förch, K. Landfester and U. Jonas, *Adv. Funct. Mater.*, 2012, **22**, 2376.
25 F. Hapiot, S. Menuel and E. Monflier, *ACS Catal.*, 2013, **3**, 1006.
26 J. E. Chung, M. Yokoyama, T. Aoyagi, Y. Sakurai and T. Okano, *J. Controlled Release*, 1998, **53**, 119.
27 J. F. Larrow, E. N. Jacobsen, Y. Gao, Y. P. Hong, X. Y. Nie and C. M. Zepp, *J. Org. Chem.*, 1994, **59**, 1939.
28 B. Roßbach, K. Leopold and R. Weberskirch, *Angew. Chem., Int. Ed.*, 2006, **45**, 1309.
29 B. Gall, M. Bortenschlager, O. Nuyken and R. Weberskirch, *Macromol. Chem. Phys.*, 2008, **209**, 1152.
30 M. J. Monteiro, *Macromolecules*, 2010, **43**, 1159.
31 M. J. Monteiro, *Macromolecules*, 2010, **43**, 9598.
32 F. Tu and D. Lee, *J. Am. Chem. Soc.*, 2014, **136**, 9999.
33 C. Baleizão and H. Garcia, *Chem. Rev.*, 2006, **106**, 3987.
34 W. Chen, Y. Sung, C. Chang, Y. Chen and M. Ger, *Surf. Coat. Technol.*, 2010, **204**, 2130.
35 L. Lou, K. Yu, F. Ding, X. Peng, M. Dong, C. Zhang and S. Liu, *J. Catal.*, 2007, **249**, 102.
36 R. Tan, D. Yin, N. Yu, H. Zhao and D. Yin, *J. Catal.*, 2009, **263**, 284.
37 R. Luo, R. Tan, Z. Peng, W. Zheng, Y. Kong and D. Yin, *J. Catal.*, 2012, **287**, 170.
38 J. Huang, X. Fu and Q. Miao, *Appl. Catal., A*, 2011, **407**, 163.
39 J. Huang, X. Fu, C. Wang, H. Zhang and Q. Miao, *Microporous Mesoporous Mater.*, 2012, **153**, 294.
40 A. R. Silva, K. Wilson, J. H. Clark and C. Freire, *Microporous Mesoporous Mater.*, 2006, **91**, 128.
41 B. Gong, X. Fu, J. Chen, Y. Li, X. Zou, X. Tu, P. Ding and L. Ma, *J. Catal.*, 2009, **262**, 9.
42 G. Liu, W. Fan, L. Li, P. K. Chu, K. W. K. Yeung, S. Wu and Z. Xu, *J. Fluorine Chem.*, 2012, **141**, 21.
43 M. Li, S. Qi, Y. Jin, W. Yao, S. Zhang and J. Zhao, *Colloids Surf., B*, 2014, **123**, 852.
44 R. Tan, D. Yin, N. Yu, Y. Jin, H. Zhao and D. Yin, *J. Catal.*, 2008, **255**, 287.
45 N. Ch. Maity, S. H. R. Abdi, R. I. Kureshy, N. H. Khan, E. Suresh, G. P. Dangi and H. C. Bajaj, *J. Catal.*, 2011, **277**, 123.
46 R. I. Kureshy, T. Roy, N. H. Khan, S. H. R. Abdi, A. Sadhukhan and H. C. Bajaj, *J. Catal.*, 2012, **286**, 41.
47 Y. Chen, R. Tan, Y. Zhang, G. Zhao, W. Zheng, R. Luo and D. Yin, *Appl. Catal., A*, 2015, **491**, 106.
48 W. Meier, *Adv. Funct. Mater.*, 2011, **21**, 1241.
49 Z. Xu, X. Ma, Y. Ma, Q. Wang and J. Zhou, *Catal. Commun.*, 2009, **10**, 1261.
50 W. Zheng, R. Tan, S. Yin, Y. Zhang, G. Zhao and D. Yin, *Catal. Sci. Technol.*, 2015, **5**, 2092.
51 C. E. Song, *Annu. Rep. Prog. Chem., Sect. C: Phys. Chem.*, 2005, **101**, 143.